



**HAL**  
open science

## Impact of erosion and décollements on large-scale faulting and folding in orogenic wedges: analogue models and case studies

Clement Perrin, Luca Clemenzi, Jacques Malavieille, Giancarlo Molli, Alfredo Taboada, Stéphane Dominguez

### ► To cite this version:

Clement Perrin, Luca Clemenzi, Jacques Malavieille, Giancarlo Molli, Alfredo Taboada, et al.. Impact of erosion and décollements on large-scale faulting and folding in orogenic wedges: analogue models and case studies. *Journal of the Geological Society*, 2013, 170 (6), pp.893-904. 10.1144/jgs2013-012 . hal-03519254

**HAL Id: hal-03519254**

**<https://hal.science/hal-03519254>**

Submitted on 10 Jan 2022

**HAL** is a multi-disciplinary open access archive for the deposit and dissemination of scientific research documents, whether they are published or not. The documents may come from teaching and research institutions in France or abroad, or from public or private research centers.

L'archive ouverte pluridisciplinaire **HAL**, est destinée au dépôt et à la diffusion de documents scientifiques de niveau recherche, publiés ou non, émanant des établissements d'enseignement et de recherche français ou étrangers, des laboratoires publics ou privés.

1  
2  
3  
4  
5  
6  
7  
8  
9  
10  
11  
12  
13  
14  
15  
16  
17  
18  
19  
20  
21  
22  
23  
24  
25  
26  
27

**Impact of erosion and décollements on  
large scale faulting and folding in orogenic wedges:  
analogue models and case studies**

**Clément Perrin <sup>a, d,\*</sup>, Luca Clemenzi <sup>a, b, c</sup>, Jacques Malavieille <sup>a</sup>,  
Giancarlo Molli <sup>b</sup>, Alfredo Taboada <sup>a</sup> and Stéphane Dominguez <sup>a</sup>.**

<sup>a</sup> Géosciences Montpellier, Université Montpellier 2, Place E. Bataillon, 34095  
Montpellier cedex 5, France

<sup>b</sup> Dipartimento di Scienze della Terra, Università di Pisa, Via S.Maria, 53, 56126 Pisa,  
Italy

<sup>c</sup> Dipartimento di Fisica e Scienze della Terra, Università degli Studi di Parma, Parco  
Area delle Scienze, 157/A 43100 Parma, Italy

<sup>d</sup> Géoazur, Université de Nice-Sophia Antipolis, Centre National de la Recherche  
Scientifique (UMR 7329), Observatoire de la Côte d'Azur, 250 av Albert Einstein,  
06560 Valbonne, France

\* Corresponding author. *Present address*: Géoazur. Université de Nice-Sophia  
Antipolis, Bât 4, 250 av Albert Einstein, Les Lucioles 1, Sophia-Antipolis 06560  
Valbonne, France. Tel.: +33 (0)4 83 61 86 82 / Fax: +33 (0)4 92 94 26 10.

E-mail address: [clement.perrin@geoazur.unice.fr](mailto:clement.perrin@geoazur.unice.fr) (C. Perrin)

5876 words (without references and captions); 114 references; 1 table; 10 figures; 2  
figures in supplementary material

Running title : Modeling erosional fold and thrust belts

28 **Abstract:** Deformation mechanisms, long-term kinematics and evolution of fold and  
29 thrust belts submitted to erosion are studied through 2D analog experiments involving  
30 large convergence. First order parameters tested include: i) décollements and/or  
31 plastic layers interbedded at different location within analog materials; ii)  
32 synconvergence surface erosion.

33 Weak layers, depending on their location in the model, favor deformation partitioning  
34 characterized by the simultaneous development of: i) underplating domains in the  
35 inner part of the wedge (basal accretion); ii) frontal accretion where the wedge grows  
36 forward. Interaction between tectonics and surface processes influence this behavior.  
37 Development of antiformal thrust stacks controlled by underplating show small- and  
38 large-scale cyclicality.

39 Thin plastic layers induce folding processes, which are studied at wedge scale.  
40 Recumbent and overturned folds, with large inverted limbs, develop in shear induced  
41 asymmetric deformation regime via progressive unrolling of synclinal hinges. Surface  
42 erosion and underplating at depth induce further rotation (passive tilting) and  
43 horizontalization of fold limbs.

44 Models results give insights to discuss the mechanisms responsible for the large-scale  
45 structures (i.e., antiformal nappe stacks, klippen and kilometer scale recumbent fold-  
46 nappes) encountered in several mountain belts such as the Montagne Noire (French  
47 Massif Central), the Galicia Variscan belt (Spain) or the Northern Apennines (Italy).

48

49

50

51

52 Orogenic wedges are characterized by complex geological structures growing and  
53 evolving over long time periods (e.g. Fossen 2010). Their building is mainly  
54 controlled by the general mechanics of subduction and by the interactions between  
55 tectonics and surface processes that modify wedge dynamics through material transfer  
56 (e.g. Malavieille 2010). Because subduction orogens suffer large convergence, the  
57 long-term deformation is intense and generates specific structures which mechanisms  
58 of genesis are still not completely understood. Among them, the way large-scale  
59 recumbent fold-nappes observed in several mountain belt forelands grow and evolve  
60 remains enigmatic (Fig. 1). The most beautiful examples in Europe are situated in the  
61 Montagne Noire (Southern French Massif Central), Galicia Mountain Belt, (Spain) or  
62 the Northern Apennines (Italy). For example, during the Variscan Orogen, large-  
63 scale fold-nappes with huge inverted limbs (sometime of more than ten kilometers of  
64 amplitude) have been created without (or with very low) metamorphism (e.g. Matte  
65 1968; Arthaud 1970). Other large scale structures are common in mountain belts, such  
66 as antiformal stacks of thrust units and subsequent frontal klippen which can be  
67 sometimes related to deformation partitioning and subsequent basal accretion of  
68 duplex structures (e.g. Elliott & Johnson 1980; Price 1981; Platt *et al.* 1985; Hatcher  
69 1989; Gutscher *et al.* 1996; Burkhard & Sommaruga 1998; Mosar 1999; Kukowski *et*  
70 *al.* 2002; Avouac 2003; Malavieille 2010; Konstantinovskaia & Malavieille 2011;  
71 Long *et al.* 2011; Webb *et al.* 2011). Basal accretion activity is generally not constant  
72 during the long-term convergent history of orogenic wedges, alternating  
73 underthrusting of new tectonic slices with the internal deformation of the already  
74 accreted ones, or even with the migration of the underplating locus to a new place.  
75 Such a cyclical underplating behavior could promote, at a whole wedge scale, an  
76 alternate change from supercritical to subcritical taper condition, in turn favoring

77 alternations between horizontal and vertical shortening observed in many orogens  
78 (e.g. Bell & Johnson, 1989; Bell & Sapkota 2012; Aerden *et al.* 2013). What  
79 mechanisms control large scale folding, basal accretion and its cyclicity remain an  
80 open question.

81

82 Analog modeling is an efficient tool to unravel the main mechanisms controlling the  
83 dynamics of orogenic wedges. Various experimental studies have investigated the  
84 influence of geometrical, kinematical and rheological parameters on the evolution of  
85 thrust wedges (see a review in Graveleau *et al.* 2012). One of the most important  
86 parameter highlighted is the layering of the accreting crustal materials that induces  
87 mechanical heterogeneity and deformation partitioning. Such a heterogeneous  
88 rheology of accreted rock sequences is the result of various factors: stratigraphy of the  
89 incoming crustal layer (e.g. Davis & Engelder 1985; Mulugeta 1988; Liu & Dixon  
90 1990; Liu *et al.* 1992; Baby *et al.* 1995; Mandal *et al.* 1997; Nieuwland *et al.* 2000;  
91 Costa & Vendeville 2002; Koyi & Vendeville 2003; Konstantinovskaia & Malavieille  
92 2005; Stockmal *et al.* 2007; Malavieille 2010; Smit *et al.* 2010), décollements in a  
93 sedimentary sequence or basement-cover interface (e.g. Konstantinovskaia &  
94 Malavieille 2011), rheological evolution of the crust due to P-T changes through time  
95 (Carry *et al.* 2009; Gueydan *et al.* 2009), or structures and fabrics inherited from an  
96 earlier tectonic history (Sutton & Watson 1986; Holdsworth *et al.* 1997; Butler *et al.*  
97 2006, 2008; Bonnet *et al.* 2007, 2008). Among the large number of previous  
98 experimental studies of thrust wedges involving multiple décollements, only a few  
99 have suggested that faults development and evolution of structures could be cyclical  
100 under specific deformation conditions (e.g. Mulugeta & Koyi 1992; Gutscher *et al.*  
101 1998a; Malavieille 2010).

102 Analog models allow to investigate the importance of surface processes (i.e. erosion  
103 and sedimentation) and their influence on the dynamics of accretionary wedges (e.g.  
104 Baby *et al.* 1995; Larroque *et al.* 1995; Storti & McClay 1995; Mugnier *et al.* 1997;  
105 McClay *et al.* 1999; Persson & Sokoutis 2002; McClay *et al.* 2004; McClay &  
106 Whitehouse 2004; Konstantinovskaia & Malavieille 2005, 2011; Graveleau &  
107 Dominguez 2008; Cruz *et al.* 2008, 2010; Malavieille 2010; Smit *et al.* 2010). Folding  
108 represents another aspect of deformation processes investigated using analog  
109 experiments but, although studied at different scales through different experimental  
110 setups (e.g. Abbassi & Mancktelow 1990; Grujic & Mancktelow 1995; Tikof &  
111 Peterson 1998; Bazalgette & Petit 2007; Noble & Dixon 2011), fold development  
112 have rarely been investigated at the scale of a whole accretionary wedge.

113

114 This study address five major questions: 1) how do décollements influence  
115 deformation partitioning within thrust wedges, and their long term evolution, 2) which  
116 mechanisms govern the development of large scale overturned folds commonly  
117 preserved in mountain belt forelands as synformal fold-nappes klippen, 3) what  
118 controls the growth of large scale antiformal structures that develop concomitantly in  
119 the hinterland, 4) what are the interactions between relatively strong plastic layers  
120 versus weak décollements, and 5) what is the impact of surface processes on all these  
121 mechanisms? We present results of an analog modeling approach that takes into  
122 account large amounts of shortening of mechanically heterogeneous, multilayered  
123 materials and simultaneous surface erosion. Our first goal is to analyze the role of  
124 strain partitioning in relation with material transfer by erosion. Then, we study the  
125 impact of thin plastic layers interlayered in the incoming material on folding  
126 mechanisms and on its evolution at the scale of a fold and thrust wedge. The main

127 experimental results are discussed and compared to large-scale tectonic structures  
128 from several mountain belts to better interpret their geometry and kinematic  
129 evolution.

130

### 131 **Experimental set up and procedure**

132 The experimental set-up simulates the basic geometry and the main mechanisms of a  
133 subduction zone where lower plate crustal materials sink beneath an upper plate. This  
134 domain of the upper-plate located above the subduction interface corresponds in the  
135 experiments to a deformable proto-forewedge equivalent to the units of the orogen  
136 already accreted, deformed and structured following subduction. All experiments are  
137 performed under normal gravity field in a classical sandbox (see Malavieille 1984 and  
138 Konstantinovskaia & Malavieille 2005, 2011), adapted to allow large shortening (over  
139 200 cm) and presenting a flexure of the basal plate taking into account the curvature  
140 of a subducting plate.

141 The sandbox (Fig. 2) is 10 cm wide and 300 cm long, with a vertical rigid buttress. At  
142 the base a thin plastic strip (dacron cloth) exits from the device through a thin slot  
143 located at the base of the buttress. It is pulled by a computer controlled step by step  
144 electric motor. Analog materials materializing the upper crust rocks of the lower plate  
145 are deposited onto the plastic strip and are dragged toward the backstop. As they  
146 cannot exit from the device, they are accreted against the upper-plate backstop. A thin  
147 layer of sand is glued on the upper surface of the plastic strip, leading to a very rough  
148 surface. It creates a high basal friction ( $\mu_b \approx 0.5$ ) between the basal strip and the  
149 analogue material of the models. According to the critical wedge theory (Davis *et al.*  
150 1983; Dahlen *et al.* 1984; Dahlen 1984), the strength of the basal décollement

151 influences the dipping of the main thrusts and backthrusts and the surface slope angle  
152 of a wedge that satisfies the yield conditions.

153

154 Three different materials are used in the models. 1) Aeolian sand, with a density of  
155 1690 kg/m<sup>3</sup>, well rounded grains, less than 300µm in size, coefficient of internal  
156 friction ( $\mu_0$ ) is 0.57 and the cohesion (C) is 100-150 Pa. It composes the upper plate  
157 protowedge and a large part of lower plate layers. 2) Glass microbeads poured in the  
158 sandcake are used to model weak layers (décollements). Diameter is 100/200 µm, and  
159 the perfect roundness of the grains leads a smaller coefficient of internal friction ( $\mu_0 =$   
160 0.44) and a negligible cohesion. 3) Plasticine is used to simulate folding because it  
161 presents a plastic behavior. It is composed by mineral oils, waxes and a solid filler  
162 made of fine powder (15µm). It does not contain water, does not dry, and can be  
163 reused. The Plasticine is melted in an oven (softening point between 39 and 42°C) and  
164 poured in a 200 x 9.8 cm mold. After cooling, 1 mm thin layers are sliced and then  
165 included in the multilayered model. To observe the final deformation of the plastic  
166 layer at the end of experiment, we have carefully cleaned the sand around the fold  
167 limbs. Practically, in the experimental procedure, when a plasticine layer is emplaced  
168 in the sand cake, the width of the thin plasticine sheet is slightly lower than the space  
169 between the two glass sidewalls to avoid parasitic effects of lateral friction along the  
170 glass. So, less than 1 mm of sand separates the plastic layer from the sidewall. As a  
171 consequence, what we can observe directly through the glass sidewall is not the  
172 plasticine layer itself, but the thin coloured sand marker which outlines its  
173 deformation.

174

175



176 Aeolian sand and glass microbeads are commonly used in physical modeling studies  
177 as analogue of upper crustal rocks with a brittle behavior. The scaling factor between  
178 their mechanical properties and those of the natural prototype is  $10^5$  (Krantz 1991;  
179 Schellart 2000; Lohrman *et al.* 2003). The same  $10^5$  scaling factor is therefore used  
180 for model dimensions (1 cm = 1 km), in order to satisfy the fundamental scaling  
181 theory for analogue modelling (Hubbert 1937, 1951; Horsfield 1977; Ramberg 1981;  
182 Davy & Cobbold 1991; Graveleau *et al.* 2011). Plasticine is a non-Newtonian fluid  
183 characterized by strain rate-dependant plastic yielding and strain hardening. At  
184 constant temperature, the constitutive flow law for plasticine is given by  $\dot{\epsilon} = C\sigma^n$ ,  
185 where  $\dot{\epsilon}$  is the strain rate, C is a material constant,  $n$  is a stress exponent, and  $\sigma$  is the  
186 differential stress (McClay 1976; Ranalli 1995). The apparent dynamic viscosity ( $\eta$ )  
187 of plasticine is given by one half the ratio between the differential stress and the strain  
188 rate:  $\eta = \sigma/(2\dot{\epsilon})$ .

189 Considering that experiments were carried at constant room temperature ( $T \sim 22$ -  
190  $25^\circ\text{C}$ ) and that the strain rate of the plasticine layer during deformation is constant  
191 and very low ( $\dot{\epsilon} \approx 1 \times 10^{-3} \text{ s}^{-1}$ ) then  $\eta \approx 4 \times 10^7 \text{ Pa s}$ . This value of viscosity was  
192 determined by mechanical experiments on plasticines (Schöpfer & Zulauf 2002;  
193 Zulauf & Zulauf 2004) whose composition is similar to the plasticine used in our  
194 analogue models.

195 The yield strength of a plasticine layer with millimetric thickness is roughly  
196 equivalent to the compressional strength of a sand layer with centimetric thickness.  
197 Thus, the strength contrast between plasticine layers and granular layers (sand or glass  
198 microbeads) in our models is roughly equivalent to the strength contrast between  
199 ductile yet strong rock layers (such as limestone) and weak rock layers (such as

200 siltstones or shale). This strength contrast is typical of sedimentary sequences  
201 observed in foreland and intra-mountainous basins in orogenic wedges.

202

203 Thirteen experiments have been run (Table 1). Among them, seven are chosen as  
204 representative to describe the main results of our study. Erosion has been applied to  
205 most of them, following the procedure described here below. First, an initial  
206 shortening without erosion is applied to the models, allowing the development of a  
207 wedge shaped topographic relief. This first step of wedge growth could be considered  
208 as the analogue of wedge development in a poorly erosional submarine setting. Then,  
209 erosion is applied step by step, each 2 cm of convergence (see digital screen in  
210 experiment pictures for shortening values), simulating a climate-dependent erosion in  
211 a subaerial wedge setting and keeping a constant evolution of the wedge topography.  
212 It is performed by scraping off all the material rising above an imposed erosion  
213 surface and then removing it with a vacuum cleaner. The slope of this erosion surface  
214 can be variable or fixed and predetermined. In the former case the slope of the erosion  
215 surface is adjusted step by step, in order to follow the “instantaneous” average slope  
216 of the wedge, just smoothing in this way the small scale irregularities of the  
217 topographic profile without altering its average slope. In the latter case an average  
218 tilted erosion profile dipping from 3 to 10° toward the foreland is maintained  
219 (Konstantinovskaia & Malavieille 2005, 2011; Bonnet *et al.* 2007, 2008). This slope  
220 corresponds to the critical taper slope of a dry sand wedge (Davis *et al.* 1983). In this  
221 case, local erosion rates are directly controlled by the activity of thrusts. Even if the  
222 role of sedimentation has not specifically been taken into account in this study, small  
223 piggy back basins that develop during wedge growth have been filled while  
224 performing erosion to avoid unrealistic foreland topographies.

225

## 226 **Experimental results**

227 Our new set of experiments complements previous modeling works on orogenic  
228 processes carried out at the Geosciences Laboratory in Montpellier, which outline the  
229 impact of coupling between surface and tectonic processes and the important role of  
230 décollement levels during deformation (see, Malavieille *et al.* 1993; Larroque *et al.*  
231 1995; Konstantinovskaia & Malavieille 2005, 2011; Bonnet *et al.* 2007, 2008;  
232 Malavieille 2010). Décollement layers favor the mechanical decoupling of stratified  
233 material of the subducting plate and consequently, induce deformation partitioning.  
234 While upper units are accreted at the toe of the wedge during propagation of the  
235 deformation front (frontal accretion), lower units are underthrusting below the main  
236 décollement fault and accreted at the base of the wedge by duplexing and  
237 underplating (i.e. basal accretion). This partition between vertical and horizontal  
238 accretion has a major impact on the organization of tectonic structures, deformation  
239 and exhumation of deep units (e.g. Gutscher *et al.* 1998; Bonini 2001, 2003; Adam *et*  
240 *al.* 2002; Kukowski *et al.* 2002; Konstantinovskaia & Malavieille 2005, 2011; Bonnet  
241 *et al.* 2007, 2008; Hoth *et al.* 2006, 2007, 2008; Malavieille 2010).

242

### 243 *Influence of weak layers*

244 A microbeads layer deposited on the top surface of the lower plate (experiment 1, Fig.  
245 3a) favors underthrusting of the tectonic units below the protowedge in the first steps  
246 of experiments. During shortening, the wedge grows mostly in sequence by frontal  
247 accretion and shows the typical structure of a simple sand wedge with no décollement  
248 in the incoming sequence. We recognize typical structures of high basal friction  
249 wedges built up by underthrusting of long tectonic units (e.g. Malavieille *et al.* 1992;

250 Lallemand *et al.* 1994; Gutscher *et al.* 1998a, 1998b; Nieuwland *et al.* 2000; Agarwal  
251 & Agrawal 2002; Kukowski *et al.* 2002; Konstantinovskaia & Malavieille 2005;  
252 Graveleau *et al.* 2012). In some cases, when the deformation front advances toward  
253 the foreland through the nucleation of a new thrust, the previous frontal thrust remains  
254 active until the end of the experiment. Internal deformation of individual forward  
255 vergent thrust units is accommodated by small backthrusts and only few large  
256 backthrusts propagate through the whole wedge.

257

258 A microbeads layer positioned at  $\sim 1/3$  of the total lower plate thickness favors  
259 remarkable strain partitioning (experiment 4, Fig. 3b). Materials of the upper portion  
260 of the subducting plate are deformed by frontal accretion, leading to the development  
261 of a typical low basal friction thrust wedge. Given the reduced thickness of the  
262 materials deformed by frontal accretion and the reduced basal friction, both the wedge  
263 taper angle (Fig. 3b) and the spacing between new thrust faults, are smaller than in  
264 experiment 1. Materials of the lower portion of the subducting plate are deformed by  
265 underplating and basal accretion (Fig. 3b). As already described in previous papers  
266 (e.g. Mulugeta & Koyi 1992; Gutscher 1996, 1998a), underplating is not a steady-  
267 state process. More in detail, it can be noted that the evolution of the duplex structure  
268 is characterized by the activity of: i) large-offset faults (continuous lines in Fig. 3b  
269 and 3c) allowing the accretion of a new unit at the base of the wedge; ii) small-offset  
270 faults (dotted lines in Fig. 3b and 3c), allowing the accommodation of the internal  
271 deformation of individual underplated units (Adam *et al.* 2002; Kukowski *et al.* 2002;  
272 Hoth *et al.* 2008). The large shortening (of the experiments presented in this paper)  
273 also allowed a second type of cyclicity to be observed at the whole-wedge scale.  
274 When the first antiformal stack of underplated units reaches a critical size, it becomes

275 inactive and the locus of underplating shifts to a more external position (e.g. toward  
276 the foreland) where a second antiformal stack starts developing. The first underplating  
277 domain is thus passively accreted and becomes part of the wedge upper-plate. Such a  
278 mechanism of accretion repeats itself cyclically during the long-term evolution of a  
279 wedge.

280 Growth of the antiformal stacks leads to some localized uplift of the overlying portion  
281 of the wedge as manifested by the shape of the topographic profile, which shows two  
282 evident bumps corresponding with the deep duplexes. By contrast the topographic  
283 profile is quite regular in wedges lacking strain partitioning (Fig. 3a and 3b).

284

285 A microbeads layer located at shallow depth in the sandcake has a slight influence on  
286 active deformation, without leading to efficient strain partitioning (experiment 6, Fig.  
287 3d). Only second order small thrust units develop along the weak layer, involving the  
288 upper portion of the subducting plate. Such small thrusts are regularly alternated with  
289 major thrusts involving the whole subducting plate, and can therefore be considered  
290 local splays of the main thrusts. The overall architecture of the wedge is that of a  
291 classical high basal friction wedge, similar to the one obtained without microbeads  
292 layer (Fig. 3d).

293

#### 294 *Influence of a plastic layer on folding*

295 In experiment 10 (Fig. 4a) the introduction of a plastic layer in the subducting plate  
296 drastically changes the tectonic style and kinematic evolution of the wedge, and leads  
297 to folding processes at the scale of a whole accretionary wedge. The main  
298 mechanisms of folds development in the experiment with no erosion are described  
299 Fig. 5. Development of folds begins by buckling of the plastic layer, which is

300 accommodated by a pop up structure in the overlying “brittle” sand layer. The  
301 wavelength of buckling and the folding mechanism are controlled by the strength  
302 contrast between the relatively strong yet ductile plasticine layer and weaker sand  
303 layers (see previous section). Soon afterwards, the folding amplitude increases, folds  
304 become asymmetric and overturned, controlled by progressive shearing deformation  
305 induced by the growth of the prism. Shearing is partly responsible for the  
306 development of the long inverted limbs, but the plastic layer is never disrupted or  
307 stretched enough to be cut, thus allowing unrolling of the synclinal hinge. Fold  
308 growth proceeds by continuous unrolling of the synclinal hinge which causes existing  
309 nearby thrusts to become inactive, while new ones form. Then, the inactive faults are  
310 passively transported along the inverted fold limb, although some can be reactivated  
311 by out-of-sequence thrusting.

312

### 313 *Impact of surface erosion*

314 The effect of surface erosion is tested on wedges characterized by different tectonic  
315 styles. In experiment 6, a simple high friction thrust wedge showing no strain  
316 partitioning or folding is submitted to erosion. It is comparable to experiment 1,  
317 except the latter did not include erosion. Figure 3d outlines the similar tectonic styles  
318 of both models, and similar taper angle of their pro-wedges.

319

320 Experiment 5 (Fig. 3c) shows the effects of erosion on a wedge characterized by  
321 strong strain partitioning, to be compared with experiment 4, which has the same  
322 initial setup but no erosion. In both models permanent underplating leads to the  
323 development of a large antiformal stack formed by basal accretion of duplex units. It  
324 induces uprising of internal domain and subsequent localized surface uplift. In model

325 5, however, surface uplift enhances localized surface erosion, which in return favors  
326 further uplift and localization of underplating. As shown in figure 3c the final product  
327 of this process is the exhumation of underplated units in localized areas.

328

329 In experiment 11 (Fig. 4b) a model involving a plastic layer is submitted to erosion in  
330 order to investigate the impact of surface processes on the dynamics of folding.  
331 Compared to experiment 10, which has the same initial setup, experiment 11 shows  
332 several differences in the general tectonic style. Despite erosion of anticlinal fold  
333 hinges, shear deformation increases the length of the inverted sequence, which is  
334 associated with the unrolling, and migration of the synclinal fold hinge. Frontal  
335 accretion spreads but the amount of shortening accommodated through each folded  
336 tectonic unit is higher. The material removed by erosion delays the growth of the  
337 wedge and thus its ability to propagate the deformation forward through new tectonic  
338 units. Although the anticline hinge is being removed by erosion, unrolling of the  
339 syncline hinge continues suggesting that the inverted limb is not submitted to traction.  
340 The diffuse shear deformation involved in the core of folds due to asymmetric  
341 shortening could be responsible for the forward migration (relative to the undeformed  
342 foreland) of the synclinal hinge.

343 To summarize the main differences, we note that each unit is more intensely deformed  
344 and that the length of fold limbs is greater in the experiment with erosion. In addition,  
345 for an equivalent amount of shortening, less tectonic units were formed.

346

#### 347 *Brittle/ductile multilayer and underplating*

348 In experiments 10 and 11, large-scale isoclinal folds developed with an average final  
349 overturning of the limbs ranging between 30° and 50°. These modeling results cannot

350 explain what is commonly observed in many natural mountain forelands where large  
351 scale inverted fold limbs rest close to horizontal over kilometers. Thus, important  
352 questions remain: what mechanism is responsible for the huge overturning observed?  
353 And, does this mechanism occur during folds development or by rigid rotation due to  
354 late tilting? In order to answer these questions, we have taken into account the  
355 insights from the experiments involving basal accretion. As previously shown,  
356 décollement layers play a key role during deformation and interactions with surface  
357 processes, that seems major too for the development of folding during the growth of  
358 fold and thrust belts.

359 In experiment 13 (Fig. 4c) we tested the impact of heterogeneous layering involving  
360 décollements, brittle and plastic behaviors (very common in foreland belts). The  
361 model combines strain partitioning, folding and surface erosion. A 5 mm thick layer  
362 of sand is placed between a 1 mm thick plasticine sheet and the 3 mm thick weak  
363 layer of glass microbeads. The complete evolution of the experiment is described in  
364 the figure 6. Erosion begins after 15 cm of shortening and the wedge slope is  
365 sustained at about 3° during shortening (60% at the end of the experiment). During  
366 convergence, fold hinges are rapidly eroded, while active thrusting occurs in the core  
367 of folds. Six folded tectonic units were obtained and a large domain of deeply  
368 accreted units is exhumed behind the prism. Note that we also observed the cyclical  
369 behavior of underplating as described previously.

370 The structures located above the décollement layer are passively deformed and  
371 uplifted due to basal accretion, tilting the back part of folded tectonic units. These  
372 deep accretionary processes are responsible for the important overturning and rotation  
373 of the flanks of folded structures. During continuous shortening, the kinematics of  
374 deformation reflects the complex interaction between wedge mechanics and erosion.



375 At the final stage most of the folded units from the backpart of the wedge have been  
376 removed by erosion. Finally, three different tectonic domains characterized by  
377 specific deformation features are juxtaposed. From the frontal part of the wedge to the  
378 backstop respectively, we have (Fig. 6): a frontal imbricate of thrust and fold sheets; a  
379 synformal klippe of folded units previously accreted to the front and progressively  
380 deformed; and, an antiformal stack of underplated thrust units refolding the upper  
381 décollement layer.

382

### 383 **Discussion and case studies**

384 Results of this series of experiments give some insights for the interpretation of  
385 several debated features of the forewedge domain of mountain belts formed in  
386 continental subduction settings. Chosen case studies are discussed in the light of our  
387 experimental results. The last model, which contains the main features described in  
388 previous sections, is used to illustrate the general mechanisms explaining the  
389 relationships between the main tectonic units of natural orogenic wedges (Fig. 7).

390

#### 391 *Examples from the Variscan Belt*

392 The Variscan orogen developed during the Gondwana-Laurasia collision from  
393 Devonian to middle Carboniferous times (e.g. Matte 2007). The Montagne Noire in  
394 southern French Massif Central and the Galicia Mountains in northwest Spain  
395 represent segments of this orogen characterized by a foreland fold and thrust belt  
396 domain associated with a syntectonic foreland basin (e.g. Arthaud 1970; Matte 1968;  
397 Pérez-Estàun *et al.* 1991; Simancas *et al.* in press). Low-grade tectonic units mainly  
398 composed by sedimentary rocks of the Paleozoic cover (schists, limestones and  
399 quartzites of Cambrian to Carboniferous ages) are intensely folded and juxtaposed

400 with antiformal stacks of Proterozoic to Cambrian metamorphic basement rock units  
401 largely exhumed in the hinterland. The Montagne Noire which forms the  
402 southernmost part of the Variscan French Massif Central (Fig. 8) is generally  
403 subdivided into three tectonostratigraphic units (e.g. Gèze 1949; Arthaud 1970). (1) A  
404 Northern Flank upper-plate unit with a southward tectonic vergence, consists of  
405 folded and faulted low-grade lower Paleozoic metasedimentary rocks. (2) An Axial  
406 Zone lower-plate unit, is formed by an antiformal structure of crystalline rocks  
407 (gneiss, migmatite, and micaschist) of Proterozoic to Ordovician age. This  
408 metamorphic domain composed by high grade rocks has been variously interpreted in  
409 terms of : diapirism (e.g. Gèze 1949; Beaud 1985 ; Charles *et al.* 2009), contractional  
410 tectonics (Arthaud *et al.* 1966; Mattauer *et al.* 1996; Aerden & Malavieille, 1999;  
411 Soula *et al.* 2001; Matte, 2007; Malavieille 2010), emplacement in a crustal scale  
412 strike-slip setting (e.g. Nicolas *et al.* 1977; Franke *et al.* 2011), or as extensional  
413 metamorphic core complex (e.g. Echtler & Malavieille, 1990; Van den Driessche &  
414 Brun 1992). In fact, most authors agree on the geological evidences for a  
415 contractional history followed (or assisted) by gravity induced extensional processes  
416 favoring exhumation, detachment formation and diapirism in the evolutionary stages  
417 of the orogen. (3) A Southern Flank, well known in the literature for the kilometer-  
418 scale recumbent fold nappes, is composed by very low-grade Paleozoic sedimentary  
419 sequences. The south verging nappes stack is intimately associated with syntectonic  
420 Viséan flysch sediments deposited in a foreland basin setting, in a shallow marine  
421 environment. The upper-plate nappes are separated from high-grade lower-plate  
422 basement units by major fault zones that record a complex pattern of deformation  
423 (e.g. Echtler & Malavieille 1990; Aerden & Malavieille 1999). Figure 8 shows an  
424 interpreted cross section of The Montagne Noire (Malavieille 2010).

425 Similar key structures of the Galicia Mountain Belt are outlined on the cross-section  
426 of figure 9, modified from Pérez-Estàun *et al.* (1991). Proterozoic metamorphic units  
427 outcrop in the internal domain while a domain of large scale recumbent folds made of  
428 Cambrian quartzite/limestone characterizes external foreland units. These kilometric  
429 scale folds present horizontal or overtilted limbs (Matte 1968; Pérez-Estàun *et al.*  
430 1991). Note that in this segment of the Variscan belt, a cyclical basal accretion may  
431 have occurred at large scale, as two antiformal stack structures formed during wedge  
432 growth.

433

434 Comparing wedges architecture and analog models, we can outline geometrical and  
435 kinematic similarities. As observed in models involving décollements and  
436 brittle/plastic behavior, there is a good analogy between the geometric configuration  
437 of the folded superficial domain and the underlying deeper structures. Where  
438 underplating develops, the folded units located above the décollement layer are  
439 strongly tilted by subsequent uplift in the antiformal stack domain. This can be  
440 compared to the fold-nappes structures of the Galicia belt or Montagne Noire. In the  
441 parts of the orogenic wedge located far from the locus of basal accretion, large scale  
442 folds are simply overturned. During the growth of the Montagne Noire, syntectonic  
443 flysches (Visean) are deposited at the toe of the wedge due to erosion of developing  
444 fold nappes (Southern flank). At the same time, basal accretion is active during the  
445 growth of the prism involving underthrusting of sliced Proterozoic basement and  
446 subsequent uplift at the back of the overturned fold domain. Already deformed Upper  
447 Paleozoic units are overtilted by progressive uplift. The décollement layer allowing  
448 strain partitioning between shallow and deep parts of the wedge is located along the

449 main inherited discontinuity, between the crystalline basement and the Paleozoic  
450 cover.

451 Figure 6 highlights the major effect of erosion on deformation processes. During  
452 wedge growth, due to combined basal accretion, surface uplift and erosion,  
453 continuous folding affects tectonic units of the upper-plate that remain at the same  
454 structural level in the upper crust whereas large domains of deep metamorphic units  
455 of the lower-plate are exhumed. Thus, the deformation mechanisms highlighted in our  
456 study may explain how the large scale recumbent fold-nappes with inverted limbs of  
457 10 km develop, and why they suffered only slight or no metamorphism.

458

#### 459 *Northern Apennines*

460 The Apennines are a fold and thrust mountain chain constituting the backbone of the  
461 Italian peninsula. Figure 10a outlines some aspects of the northernmost portion of this  
462 chain (e.g. Molli 2008). The internal zone is characterized by a metamorphic core  
463 where two main exhumed tectonostratigraphic units outcrop. The lowermost is the  
464 Apuane unit, a low grade metamorphic unit showing greenschist assemblages  
465 (deepest estimated burial: ~ 20 km). On the western side of the core, the Apuane unit  
466 is overlaid by the Massa unit, an HP greenschist facies metamorphic unit with higher  
467 grade P/T peak conditions (estimated deepest burial: ~ 25/30 km). The whole  
468 metamorphic core is overlaid by the Tuscan Nappe, an anchimetamorphic unit with a  
469 deepest estimated burial of ~ 7 km, which in turn is overlaid by Subligurian and  
470 Ligurian non-metamorphic units and by the Epiligurian basin (e.g. Fellin *et al.* 2007  
471 and references therein). In a central portion, east of the Alpi Apuane, the chain is  
472 characterized by a recumbent fold domain (Fig. 10b) where the Tuscan Nappe is  
473 folded in a kilometric-scale recumbent structure (the Val di Lima fold), with an

474 outcropping kilometers long inverted limb. This recumbent fold shows minor  
475 structures related with superimposed deformations (Baldacci *et al.* 1992; Fazzuoli *et*  
476 *al.* 1998) with development of the long inverted limb by progressive hinge migration  
477 (Botti *et al.* 2010).

478 The overall geometrical configuration of the analyzed segment of the Apennines (Fig.  
479 10) can be interpreted in the light of our models. The combined action of basal  
480 accretion and underplating of tectonic units produced the growth of a syn-  
481 metamorphic antiformal stack (Molli & Vaselli 2006) responsible of strong uplift and  
482 exhumation by submarine (in the early stages) and later surface erosion (Molli *et al.*  
483 2002; Fellin *et al.* 2007). Erosion-processes were associated with tectonic thinning by  
484 normal-slip reactivation of the basal thrust of the unmetamorphic units at the hanging  
485 wall and the metamorphic core at the footwall (Carmignani & Kligfield 1990; Molli *et*  
486 *al.* 2002; Fellin *et al.* 2007; Molli 2008). Moreover, the growth of the antiformal stack  
487 may have induced progressive tilting of the basal detachment and the formation of  
488 recumbent geometry of the folded Tuscan unit in the Lima Valley (Fig.10a,b).

489 Indeed, the locus of basal accretion and the folded domain are close enough to  
490 presume the influence of the underlying deep structures on the passive rotation of the  
491 fold limbs. Model results can give some more hints on the processes that may have  
492 influenced the geological evolution of the metamorphic core, suggesting that two  
493 successive episodes of underplating, could have been responsible for the syn-  
494 contractional juxtaposition of the Massa unit above the Apuan unit.

495

#### 496 *Open questions in other mountain belts*

497 Mechanisms responsible for deformation structures and exhumation processes  
498 developed in the Himalayas are presently widely discussed through two main kind of

499 models (ductile channel flow, e.g. Nelson *et al.* 1996; Beaumont *et al.* 2001; Jamieson  
500 *et al.* 2004; and wedge extrusion in a thrust system, e.g. Burchfiel & Royden 1985;  
501 England & Molnar 1993; Guillot & Allemand 2002, Webb *et al.* 2007, Kali *et al.*  
502 2010). Our study outline simple mechanisms that seem to be consistent with the  
503 observed large-scale geological structures (antiformal stacks, synformal klippen of  
504 fold and thrust units), in agreement with the second orogenic wedge model.

505

## 506 **Conclusions**

507 Interaction between climate controlled surface processes including erosion,  
508 sedimentation and deformation processes plays a key role in the structural evolution,  
509 kinematics and exhumation of rocks in orogenic wedges. During continental  
510 subduction, the role of the rheologic layering of the crust can be major as it  
511 determines the partitioning of deformation in a growing orogenic wedge into domains  
512 undergoing horizontal and vertical accretion. Partitioning is first controlled by  
513 tectonic processes, but material transfer induced by surface processes exerts a strong  
514 feed-back on wedge dynamics. Insights from analog models applied to natural cases  
515 allow us to emphasize several first order interaction mechanisms that result from this  
516 coupling. Experiments show that strain partitioning is not systematic but depends on  
517 the position of weak layers in the layered incoming sequence. They show a cyclical  
518 behavior of basal accretion, leading to episodic underplating of tectonic units, which  
519 has a strong impact on the vertical component of displacement of rock material. In  
520 turn, it changes surface slopes favoring erosion in domains of strong surface uplift. In  
521 addition, our experiments offer an explanation for the enigmatic domains of non  
522 metamorphic large scale fold nappes units observed in the foreland of many orogenic  
523 wedges. To a first order, the dynamics of folding involves rolling of a synclinal hinge

524 and develop exclusively overturned fold types. This mechanism was observed, in  
525 particular, for multilayered models constituted of both strong yet ductile layers and  
526 comparatively weaker granular layers.

527 The influence of the deep wedge dynamics, such as the growth of basal duplexes,  
528 causes further rotation of fold structures, leading to the horizontalization of fold  
529 limbs, while erosion processes keep the folded units in a superficial low-grade  
530 metamorphic domain. Natural wedges (e.g. Galicia, Montagne Noire and Northern  
531 Apennines) present close similarities to the experiments described herein, both in  
532 terms of architecture and orogenic dynamics. Other orogenic wedges exposing similar  
533 structures such as exhumed antiformal metamorphic domes juxtaposed with domains  
534 of largely folded upper-crustal rock sequences need to be revisited in the light of the  
535 general mechanisms here outlined.

536 Future work should concentrate on multilayered models with different rheological  
537 contrasts (e.g. weak ductile layers and strong brittle layers) to determine other  
538 possible large-scale folding mechanisms in the shallow domains of orogenic wedges.

539

540

#### 541 **Acknowledgements**

542 Our modeling work has benefitted from the technical assistance of C. Romano. Many  
543 thanks to Nina Kukowski who helped us improving an early version of the  
544 manuscript. This study has been partly funded in the frame of the ACTS ANR project.

545 The contribution by Clemenzi has benefitted from an Erasmus Placement exchange  
546 and funding between Pisa and Montpellier Universities. This paper benefitted from  
547 constructive review by D.G.A.M. Aerden and an anonymous reviewer.

548

549

550 **References**

551 ABBASSI, M. R. & MANCKTELOW, N. S. 1990. The effect of initial perturbation shape  
552 and symmetry on fold development. *Journal of Structural Geology*, **12**, 273–282.

553

554 ADAM, J., LOHRMANN, J., HOTH, S., KUKOWSKI, N. & ONCKEN, O. 2002. Strain  
555 variation and partitioning in thrust wedges: high-resolution data from scaled sandbox  
556 experiments by 2D–3D PIV analysis. *Bollettino di Geofisica Teorica ed Applicata*,  
557 **42**, 123–125.

558

559 AERDEN, D. G. A. M. & MALAVIEILLE, J. 1999. Origin of a large-scale fold nappe in  
560 the Montagne Noire, Variscan belt, France. *Journal of Structural Geology*, **21**, 1321–  
561 1333.

562

563 AERDEN, D. G. A. M., BELL, T. H., PUGA, E., SAYAB, M., LOZANO, J. A. & DIAZ DE  
564 FEDERICO, A. 2013. Multi-stage mountain building vs. relative plate motions in the  
565 Betic Cordillera deduced from integrated microstructural and petrological analysis of  
566 porphyroblast inclusion trails. *Tectonophysics*, **587**, 188–206

567

568 AGARWAL, K. K. & AGRAWAL, G. K. 2002. Analogue sandbox models of thrust  
569 wedges with variable basal frictions. *Gondwana Research*, **5**, 641–647.

570

571 ARTHAUD, F. 1970. Etude tectonique et microtectonique comparée de deux domaines  
572 Hercyniens : les nappes de la Montagne Noire (France) et l'anticlinorium de l'Iglesiente  
573 (Sardaigne). *Publications de l'université des Sciences et Techniques du Languedoc*,



574 *Montpellier. Série Géologie Structurale, 1.*

575

576 ARTHAUD, F., MATTAUER, M. & PROUST, F. 1966. La structure et la microtectonique  
577 des nappes hercyniennes de la Montagne Noire. Colloque “Étages Tectoniques”,  
578 Neuchâtel, 231–247.

579

580 AVOUAC, J. P. 2003. Mountain Building, Erosion, and the Seismic Cycle in the Nepal  
581 Himalaya. *In: Advances in Geophysics*, Elsevier, **46**, 1-80.

582

583 BABY, P., COLLETTA, B. & ZUBIETA, D. 1995. Etude géométrique et expérimentale  
584 d'un bassin transporté: exemple du synclinorium de l'Alto Beni (Andes centrales).  
585 *Bulletin de la Société Géologique de France*, **166**, 797-811.

586

587 BALDACCI, F., CARMIGNANI, L., FANTOZZI, P., MECCHERI, M. & PLESI, G. 1992.  
588 Lineamenti stratigrafico-strutturali lungo la trasversale Alpi Apuane - Appennino  
589 reggiano-modenese. *Studi Geol. Camerti*, Vol. Spec., 31-49.

590

591 BAZALGETTE, L. & PETIT, J. P. 2007. Fold amplification and style transition involving  
592 fractured dip-domain boundaries: buckling experiments in brittle paraffin wax  
593 multilayers and comparison with natural examples. *In: LONERGAN, L., JOLLY, R.J.H.,*  
594 *RAWNSLEY, K. & SANDERSON, D. J. (eds) Fractured Reservoirs*. Geological Society,  
595 London, Special Publications, **270**, 157–169.

596

597 BEAUD, F. 1985. Etude structurale de la Zone Axiale orientale de la Montagne Noire  
598 (Sud du Massif Central Français). Détermination des mécanismes de déformation.

599 Relation avec les nappes du Versant Sud. Thèse 3ème cycle, Université des Sciences  
600 et Techniques du Languedoc, Montpellier, 191 p.

601

602 BEAUMONT, C., JAMIESON, R. A., NGUYEN M. H. & LEE, B. 2001. Himalayan tectonics  
603 explained by extrusion of a low-viscosity crustal channel coupled to focused surface  
604 denudation, *Nature*, **414**, 738–742, doi:10.1038/414738a

605

606 BELL, T. H. & JOHNSON, S. E. 1989. Porphyroblast inclusion trails: the key to  
607 orogenesis. *Journal of Metamorphic Geology*. **7**, 279–310, doi:10.1111/j.1525-  
608 1314.1989.tb00598.x

609

610 BELL, T. H. & SAPKOTA, J. 2012. Episodic gravitational collapse and migration of the  
611 mountain chain during orogenic roll-on in the Himalayas. *Journal of Metamorphic  
612 Geology*, **30**, 651–666, doi: 10.1111/j.1525-1314.2012.00992.x

613

614 BONINI, M. 2001. Passive roof thrusting and forelandward fold propagation in scaled  
615 brittle-ductile physical models of thrust wedges. *Journal of Geophysical Research*,  
616 **106**(B2), 2291-2311.

617

618 BONINI, M. 2003. Detachment folding, fold amplification, and diapirism in thrust  
619 wedge experiments. *Tectonics*, **22**(6): 1065.

620

621 BONNET, C., MALAVIEILLE, J. & MOSAR, J. 2007. Interactions between tectonics,  
622 erosion, and sedimentation during the recent evolution of the Alpine orogen:  
623 Analogue modeling insights. *Tectonics*, **26**, TC6016, doi : 10.1029/2006TC002048.

624

625 BONNET, C., MALAVIEILLE, J. & MOSAR, J. 2008. Surface processes versus kinematics  
626 of thrust belts: impact on rates of erosion, sedimentation, and exhumation – Insights  
627 from analogue models. *Bulletin de la Société Géologique de France*, **179**, 179-192.

628

629 BOTTI, F., DANIELE, G., BALDACCI, F. & MOLLI, G. 2010. Note Illustrative della Carta  
630 Geologica d'Italia alla scala 1: 50.000, Foglio 251 Porretta Terme. *Servizio Geologico*  
631 *d'Italia, Regione Emilia-Romagna*.

632

633 BURCHFIEL, B. C. & ROYDEN, L. H., 1985. North-south extension within the  
634 convergent Himalayan region, *Geology*, **13**, 679–682

635

636 BURKHARD, M. & SOMMARUGA, A. 1998. Evolution of the western Swiss Molasse  
637 basin: structural relations with the Alps and the Jura belt. *In*: MASCLE, A,  
638 PUIGDEFABREGAS, C., LUTERBACHER, H.P. & FERNANDEZ, M. (eds) *Cenozoic*  
639 *Foreland Basins of Western Europe*. Geological Society, London, Special  
640 Publications, **134**, 279-298.

641

642 BUTLER, R. W. H., TAVARNELLI, E. & GRASSO, M. 2006. Structural inheritance in  
643 mountain belts : An Alpine-Apennine perspective. *Journal of Structural Geology*, **28**,  
644 1893–1908.

645

646 BUTLER, R. W. H., BOND, C. E., SHIPTON, Z. K., JONES, R. R. & CASEY, M. 2008.  
647 Fabric anisotropy controls faulting in the continental crust. *Journal of the Geological*  
648 *Society, London*, **165**, pp. 449–452.

649

650 CARMIGNANI, L. & KLIGFIELD, R. 1990. Crustal extension in the Northern Apennines:  
651 the transition from compression to extension in the Alpi Apuane Core Complex.  
652 *Tectonics*, **9**, 1275-1303.

653

654 CARRY, N., GUEYDAN, F., BRUN, J. P. & MARQUER, D. 2009. Mechanical decoupling  
655 of high-pressure crustal units during continental subduction. *Earth and Planetary  
656 Science Letters*, **278**, 13–25.

657

658 CHARLES, N., FAURE, M., AND CHEN, Y. 2009. The Montagne Noire migmatitic dome  
659 emplacement (French Massif Central): new insights from petrofabric and AMS  
660 studies. *Journal of Structural Geology*, **31**, 1423–1440, doi:10.1016/j.jsg.2009.08.007

661

662 COSTA, E. & VENDEVILLE, B. E. 2002. Experimental insights on the geometry and  
663 kinematics of fold-and-thrust belts above weak, viscous evaporitic décollement.  
664 *Journal of Structural Geology*, **24**, 1729–1739.

665

666 CRUZ, L., TEYSSIER, T., PERG, L., TAKE, A. & FAYON, A. 2008. Deformation,  
667 exhumation, and topography of experimental doubly-vergent orogenic wedges  
668 subjected to asymmetric erosion. *Journal of Structural Geology*, **30**, 98–115.

669

670 CRUZ, L., MALINSKI, J., WILSON, A., TAKE, W. A. & HILLEY, G. 2010. Erosional  
671 control of the kinematics and geometry of fold- and- thrust belts imaged in a physical  
672 and numerical sandbox. *Journal of Geophysical Research*, **115**, B09404,  
673 doi:10.1029/2010JB007472.

674

675 DAHLEN, F.A. 1984. Non cohesive critical coulomb wedges: an exact solution.  
676 *Journal of Geophysical Research*, **89**, 10125-10133.

677

678 DAHLEN, F. A., SUPPE, J. & DAVIS, D. 1984. Mechanics of fold-and-thrust belts and  
679 accretionary wedges: cohesive coulomb theory. *Journal of Geophysical Research*, **89**,  
680 10087-10101.

681

682 DAVIS, D., SUPPE, J. & DAHLEN, F. A. 1983. Mechanics of fold-and-thrust belts and  
683 accretionary wedges. *Journal of Geophysical Research*, **88**, 1153-1172.

684

685 DAVIS, D. & ENGELDER T. 1985. The role of salt in fold-and-thrust belts.  
686 *Tectonophysics*, **119**, 67–88

687

688 DAVY, P. & COBBOLD, P. R. 1991. Experiments on shortening of a 4-layer model of  
689 the continental lithosphere. *Tectonophysics*, **188**, 1-25.

690

691 ECHTLER, H., & MALAVIEILLE, J. 1990. Extensional tectonics, basement uplift and  
692 Stephano- Permian collapse basin in a late Variscan metamorphic core complex  
693 (Montagne Noire, southern Massif Central). *Tectonophysics*, **177**, 125–138.

694

695 ENGLAND, P., & MOLNAR, P. 1993. Cause and effect among thrust and normal  
696 faulting, anatectic melting and exhumation in the Himalaya. In: TRELOAR, P. J.,  
697 SEARLE, M. P. (Eds.), *Himalayan Tectonics*. Geological Society, London, Special  
698 Publications, **74**, 401–411.

699

700 ELLIOTT, D., & JOHNSON, M. R. W. 1980. Structural evolution in the northern part of  
701 the Moine thrust belt, NW Scotland. *Edinburgh Geological Society Transactions,*  
702 *Earth Sciences*, **71**, 69–96.

703

704 FAZZUOLI, M., BECARELLI, S., BURCHIETTI, G., FERRINI, G., GARZONIO, C.A.,  
705 MANNORI, G., SANI, F. & SGUAZZONI, G. 1998. Geologia del nucleo Mesozoico della  
706 Val di Lima (Province di Pistoia e Lucca, Appennino settentrionale). Note illustrative  
707 della carta geologica (Scala 1: 25.000). *Bollettino della Società Geologica Italiana*,  
708 **117**, 479-535.

709

710 FELLIN, M. G., REINERS, P. W., BRANDON, M. T., WÜTHRICH, E., BALESTRIERI M. L. &  
711 MOLLI, G. 2007. Thermochronologic evidence for the exhumational history of the  
712 Alpi Apuane metamorphic core complex, northern Apennines, Italy. *Tectonics*, **26**,  
713 TC6015, doi:10.1029/2006TC002085

714

715 FOSSEN, H. 2010. *Structural Geology*, Cambridge University Press, 463 pp., ISBN-13  
716 978-0-521-51664-8

717

718 FRANKE, W., DOUBLIER, M. P., KLAMA, K., POTEL, S. & WEMMER, K. 2011. Hot  
719 metamorphic core complex in a cold foreland. *International Journal of Earth*  
720 *Sciences*, **100**, 753-785, doi:10.1007/s00531-010-0512-7.

721

722 GÈZE, B. 1949. Etude géologique de la Montagne Noire et des Cévennes  
723 méridionales. *Mémoires de la société géologique de France*, **62**, 1–215.

724

725 GRAVELEAU, F. & DOMINGUEZ, S. 2008. Analogue modelling of the interaction  
726 between tectonics, erosion and sedimentation in foreland thrust belts. *C.R.*  
727 *Géoscience*, **340**, 324–333

728

729 GRAVELEAU, F., HURTREZ, J.-E., DOMINGUEZ, S. & MALAVIEILLE, J. 2011. A new  
730 experimental material for modeling relief dynamics and interactions between tectonics  
731 and surface processes. *Tectonophysics*, **513**, 68-87.

732

733 GRAVELEAU, F., MALAVIEILLE, J. & DOMINGUEZ, S. 2012. Experimental modelling of  
734 orogenic wedges: A review. *Tectonophysics*, **538**, 1-66.

735

736 GRUJIC, D. & MANCKTELOW, N.S. 1995. Folds with axes parallel to the extension  
737 direction: an experimental study. *Journal of Structural Geology*, **17**, 279-291

738

739 GUEYDAN, F., LE GARZIC, E. & CARRY, N. 2009. P/T ratio in high-pressure rocks as a  
740 function of dip and velocity of continental subduction. *Lithosphere*, **1**, 282–290.

741

742 GUILLOT, D., & ALLEMAND, P. 2002. Two dimensional thermal modelling of the early  
743 tectonometamorphic evolution in central Himalaya, *Journal of Geodynamics*, **34**, 77–  
744 98, doi:10.1016/S0264-3707(02)00016-9.

745

746 GUTSCHER, M. A., KUKOWSKI, N., MALAVIEILLE, J. & LALLEMAND, S. 1996. Cyclical  
747 behavior of thrust wedges: Insights from high basal friction sandbox experiments.  
748 *Geology*, **24**, 135-138.

749

750 GUTSCHER, M. A., KUKOWSKI, N., MALAVIEILLE, J. & LALLEMAND, S. 1998a.  
751 Episodic Imbricate thrusting & underthrusting; Analog experiments and Mechanical  
752 Analysis applied to the Alaskan Accretionary Wedge. *Journal of Geophysical*  
753 *Research.*, **103**, 10161-10176.

754

755 GUTSCHER, M. A., KUKOWSKI, N., MALAVIEILLE, J. & LALLEMAND, S. 1998b.  
756 Material transfer in accretionary wedges from analysis of a systematic series of analog  
757 experiments. *Journal of Structural Geology*, **20**, 407–416.

758

759 HATCHER JR, R. D. 1989. Tectonic synthesis of the U.S. Appalachians. *In*: HATCHER,  
760 R.D., THOMAS, W.A., AND VIELE, G.W. (eds), *The Appalachian-Ouachita Orogen in*  
761 *the United States : Boulder, Colorado*. The Geology of North America, **F-2**, 511–535.

762

763 HOLDSWORTH, R. E., BUTLER, C. A. & ROBERTS, A. M. 1997. The recognition of  
764 reactivation during continental deformation. *Journal of the Geological Society*,  
765 *London*, **154**, 73–78.

766

767 HORSFIELD, W. 1977. An experimental approach to basement-controlled faulting.  
768 *Geologie en Mijnbouw*, **56**, 363-370.

769

770 HOTH, S., ADAM, J., KUKOWSKI, N. & ONCKEN, O. 2006. Influence of erosion on the  
771 kinematics of bivergent orogens. Results from scaled sandbox simulations. *In*:  
772 WILLETT, S.D., HOVIUS, N., BRANDON, M.T., FISHER, D.M. (eds), *Tectonics, Climate,*  
773 *and Landscape Evolution*. The Geological Society of America, Boulder, Colorado,



774 Special Paper, **398**, 201–225.

775

776 HOTH, S., HOFFMANN-ROTHER, A. & KUKOWSKI, N. 2007. Frontal accretion: an internal  
777 clock for bivergent wedge deformation and surface uplift. *Journal of Geophysical*  
778 *Research*, **112**, B06408. doi:10.1029/2006JB004357.

779

780 HOTH, S., KUKOWSKI, N. & ONCKEN, O. 2008. Distant effects in bivergent orogenic  
781 belts—how retro-wedge erosion triggers resource formation in pro-foreland basins.  
782 *Earth and Planetary Science Letters*, **273**(1–2), 28–37.

783

784 HUBBERT, M. K. 1937. Theory of scale models as applied to the study of geologic  
785 structures. *Bulletin of the Geological Society of America*, **48**, 1459-1519.

786

787 HUBBERT, M. K. 1951. Mechanical basis for certain familiar geologic structures.  
788 *Bulletin of the Geological Society of America*, **62**, 355-372.

789

790 JAMIESON, R. A., BEAUMONT, C., MEDVEDEV, S. & NGUYEN, M. H. 2004. Crustal  
791 channel flows: 2. Numerical models with implications for metamorphism in the  
792 Himalayan-Tibetan orogen, *Journal of Geophysical Research*, **109**, B06407,  
793 doi:10.1029/2003JB002811.

794

795 KALI, K. E., LELOUP, P. H., ARNAUD, N., MAHEO, G., DUNYI LIU, BOUTONNET, E.,  
796 VAN DER WOERD, J., XIAOHAN LIU, JING LIU-ZENG, AND HAIBING LI 2010.  
797 Exhumation history of the deepest central Himalayan rocks, Ama Drime range: Key  
798 pressure-temperature-deformation-time constraints on orogenic models. *Tectonics*,

799 **29**, TC2014, doi:10.1029/2009TC002551

800

801 KONSTANTINOVSKAIA, E. & MALAVIEILLE, J. 2005. Erosion and exhumation in  
802 accretionary orogens: Experimental and geological approaches. *Geochemistry,*  
803 *Geophysics, Geosystems*, **6**, Q02006, doi:10.1029/2004GC000794, ISSN: 1525-2027

804

805 KONSTANTINOVSKAIA, E. & MALAVIEILLE, J. 2011. Thrust wedges with décollement  
806 levels and syntectonic erosion: A view from analogue models. *Tectonophysics*, 502  
807 336–350, 10.1016/j.tecto.2011.01.020.

808

809 KOYI, H. A. & VENDEVILLE, B. C. 2003. The effect of décollement dip on geometry  
810 and kinematics of model accretionary wedges. *Journal of Structural Geology*, **25**,  
811 1445-1450.

812

813 KRANTZ, R. W. 1991. Measurements of friction coefficients and cohesion for faulting  
814 and fault reactivation in laboratory models using sand and sand mixtures.  
815 *Tectonophysics*, **188**, 203-207.

816

817 KUKOWSKI, N., LALLEMAND, S., MALAVIEILLE, J., GUTSCHER, M.A. & RESTON T.J.  
818 2002. Mechanical decoupling and basal duplex formation observed in sandbox  
819 experiments with application to the Western Mediterranean Ridge accretionary  
820 complex. *Marine Geology*, **186**, 29–42

821

822 LALLEMAND, S., SCHNURLE, P. & MALAVIEILLE, J. 1994. Coulomb theory applied to  
823 accretionary and non-accretionary wedges - Possible causes for tectonic erosion

824 and/or frontal accretion. *Journal of Geophysical Research*, **99**(B6), 12033-12055.

825

826 LARROQUE, C., CALASSOU, S., MALAVIEILLE, J. & CHANIER, F. 1995. Experimental  
827 modelling of forearc basin development during accretionary wedge growth. *Basin*  
828 *Research*, **7**(3), 255–268.

829

830 LIU, S. & DIXON, M. 1990. Centrifuge modelling of thrust faulting: strain partitioning  
831 and sequence of thrusting in duplex structures. *Geological Society, London, Special*  
832 *Publications*. **54**, 431-444.

833

834 LIU, H., MCCLAY, K. & POWELL, D. 1992. Physical models of thrust wedges. *In*:  
835 MCCLAY K. (ed) *Thrust Tectonics*. Chapman and Hall, London, 71-81.

836

837 LOHRMAN, J., KUKOWSKI, N., ADAM, J. & ONCKEN, O. 2003. The impact of analogue  
838 material properties on the geometry, kinematics, and dynamics of convergent sand  
839 wedges. *Journal of Structural Geology*, **25**, 1691–1711.

840

841 LONG, S., MCQUARRIE, N., TOBGAY, T. & HAWTHORNE, J. 2011. Quantifying internal  
842 strain and deformation temperature in the eastern Himalaya, Bhutan: Implications for  
843 the evolution of strain in thrust sheets. *Journal of Structural Geology*, **33**, doi:  
844 10.1016/j.jsg.2010.12.011

845

846 MALAVIEILLE, J. 1984. Modélisation expérimentale des chevauchements imbriqués:  
847 Application aux chaînes de montagnes. *Bulletin de la Société Géologique de France*,  
848 **26**, 129–138.

849

850 MALAVIEILLE, J. 2010. Impact of erosion, sedimentation, and structural heritage on  
851 the structure and kinematics of orogenic wedges: Analog models and case studies.

852 *GSA Today*, **20**, doi: 10.1130/GSATG48A.1

853

854 MALAVIEILLE, J., CALASSOU, S., LALLEMAND, S. & LARROQUE, C. 1992. Experimental  
855 modeling of accretionary wedges. Série cours M037, Produced and realized by  
856 SNEA(P), France, 28 min.

857

858 MALAVIEILLE, J., LARROQUE, C., CALASSOU, S. 1993. Modelisation experimentale des  
859 relations tectonique/sedimentation entre bassin avant-arc et prisme d'accretion.

860 *Comptes rendus de l'Académie des sciences*, **316**, 8, 1131-1137

861

862 MANDAL, N., CHATTOPHDHYAY, A. & BOSE, S. 1997. Imbricate thrust spacing:  
863 experimental and theoretical analyses. *In: SENGUPTA, S. (ed) Evolution of Geologic*  
864 *Structures in Micro to Macro-scale*. Chapman & Hall, London, 143-165.

865

866 McCLAY, K. 1976. The rheology of plasticine. *Tectonophysics*, **33**, T7– T15.

867

868 McCLAY, K., DOOLEY, T. & WHITEHOUSE O. 1999. Analogue modelling of thin and  
869 thick-skinned thrust systems, Thrust Tectonics Conference, Paper **18**, p 45. Geology  
870 Department, Royal Holloway University of London, Egham, England.

871

872 McCLAY, K. R., WHITEHOUSE, P. S., DOOLEY, T. & RICHARDS, M. 2004. 3D evolution  
873 of fold and thrust belts formed by oblique convergence. *Marine and Petroleum*

874 *Geology*, **21**, 857-877.

875

876 MCCLAY, K. R. & WHITEHOUSE, P. S. 2004. Analog Modeling of Doubly Vergent  
877 Thrust Wedges. *In*: MCCLAY, K. (ed) *Thrust tectonics and hydrocarbon systems*.  
878 AAPG Memoir, **82**, 184–206.

879

880 MATTE, P. 1968. La structure de la virgation hercynienne de Galice (Espagne).  
881 *Géologie Alpine*, **44**.

882

883 MATTE, P. 2007. Variscan thrust nappes, detachments, and strike-slip faults in the  
884 French Massif Central: Interpretation of the lineations. *In*: HATCHER JR., R.D.,  
885 CARLSON, M.P., MCBRIDE, J.H. & MARTÍNEZ CATALÁN, J.R. (eds), *4-D Framework of*  
886 *Continental Crust*. Geological Society of America, Memoir, **200**, 391–402. Doi:  
887 10.1130/2007.1200(20)

888

889 MOLLI, G. 2008. Northern Apennine-Corsica orogenic system: an updated overview.  
890 *In*: SIEGSMUND, S., FUGENSCHUH, B. & FROITZHEIM, N. (eds) *Tectonic Aspects of the*  
891 *Alpine-Dinaride-Carpathian System*. Geological Society, London, Special  
892 Publications, **298**, 413–442

893

894 MOLLI, G. & VASELLI, L. 2006. Structures, interference patterns and strain regime  
895 during mid-crustal deformation in the Alpi Apuane (Northern Apennine, Italy),  
896 *Geological Society of America*, Special Paper, 414, 79-93

897

898 MOLLI, G., GIORGETTI, G. & MECCHERI, M. 2002. Tectono-metamorphic evolution of

899 the Alpi Apuane Metamorphic Complex: new data and constraints for geodynamic  
900 models. *Bollettino della Società Geologica Italiana*, volume speciale n.1, 789-800.

901

902 MOSAR J. 1999. Present-day and future tectonic underplating in the Western  
903 SwissAlps: reconciliation of basement/wrench-faulting and décollement folding of the  
904 Jura and Molasse Basin in the Alpine foreland. *Earth and Planetary Science Letters*,  
905 **173/3**, 143-155.

906

907 MUGNIER, J. L., BABY, P., COLLETTA, B., VINOUR, P., BALE, P. & LETURMY, P. 1997.  
908 Thrust geometry controlled by erosion and sedimentation: A view from analogue  
909 models. *Geology*, **25**, 427–430.

910

911 MULUGETA, G. 1988. Modelling the geometry of Coulomb thrust wedges. *Journal of*  
912 *Structural Geology*, **10**, 847-859.

913

914 MULUGETA, G. & KOYI, H. 1992. Episodic accretion and strain partitioning in a model  
915 sand wedge. *Tectonophysics*, **202**, 319-333.

916

917 NELSON, K. D., et al. 1996. Partially molten middle crust beneath southern Tibet:  
918 Synthesis of project INDEPTH results, *Science*, **274**, 1684–1688,  
919 doi:10.1126/science.274.5293.1684.

920

921 NICOLAS, A., BOUCHEZ, J. L., BLAISE, J. L. & POIRIER, J. P. 1977. Geological aspects  
922 of deformation in continental shear-zones. *Tectonophysics*, **42**, 55-73, doi:  
923 10.1016/0040-1951(77)90017-8.

924

925 NIEUWLAND, D. A., LEUTSCHER, J. H. & GAST, J. 2000. Wedge equilibrium in fold-  
926 and-thrust belts: prediction of out-of-sequence thrusting based on sandbox  
927 experiments and natural examples. *Netherlands Journal of Geosciences*, **79**, 81-91.

928

929 NOBLE, T. E. & DIXON, J. M. 2011. Structural evolution of fold-thrust structures in  
930 analog models deformed in a large geotechnical centrifuge. *Journal of Structural*  
931 *Geology*, **33**, 62–77

932

933 PÉREZ-ESTÀUN, A., MARTINEZ-CATALAN, J. R. & BASTIDA, F. 1991. Crustal  
934 thickening and deformation sequence in the footwall to the suture of the Variscan belt  
935 of NW Spain. *Tectonophysics*, **191**, 243–253

936

937 PERSSON, K. S. & SOKOUTIS, D. 2002. Analogue models of orogenic wedges  
938 controlled by erosion. *Tectonophysics*, **356**, 323-336.

939

940 PLATT, J. P., LEGGETT, J. K., YOUNG, J., RAZA, H. & ALAM, S. 1985. Large-scale  
941 sediment underplating in the Makran accretionary prism, southwest Pakistan:  
942 *Geology*, **13**, 507–511.

943

944 PRICE, R. A. 1981. The Cordilleran foreland thrust and fold belt in the southern  
945 Canadian Rocky Mountains. *In*: MCCLAY, K. & PRICE, N.J. (eds) *Thrust and nappe*  
946 *tectonics*. Geological Society, London, Special Publication, **9**, 427–448.

947

948 RAMBERG, H. 1981. *Gravity, deformation and the earth's crust*, 2nd edition,

949 Academic press, London. 452 pp.

950

951 RANALLI, G. 1995. *Rheology of the Earth*, 2nd edition, Chapman & Hall, London.

952

953 SCHELLART, W. P. 2000. Shear test results for cohesion and friction coefficients for  
954 different granular materials: scaling implications for their usage in analogue  
955 modelling. *Tectonophysics*, **324**, 1-16

956

957 SCHÖPFER, M. P. J. & ZULAUF, G., 2002. Strain dependent rheology and the memory  
958 of plasticine. *Tectonophysics*, **354**, 85–99.

959

960 SIMANCAS, J. F., AYARZA, P., AZOR, A., CARBONELL, R., MARTINEZ POYATOS, D.,  
961 PÉREZ-ESTÀUN, A., GONZALEZ LODEIRO, F. A. A seismic geotraverse across the  
962 Iberian Variscides: orogenic shortening, collisional magmatism and orocline  
963 development. *Tectonics*, *in press*, doi : 10.1002/tect.20035

964

965 SMIT, J., BURG, J.-P., DOLATI, A. & SOKOUTIS, D. 2010. Effects of mass waste events  
966 on thrust wedges: Analogue experiments and application to the Makran accretionary  
967 wedge. *Tectonics*, **29**. TC3003, doi : 10.1029/2009TC002526

968

969 SOULA, J. C., DEBAT, P., BRUSSET, S., BESSIÈRE, G., CHRISTOPHOUL, F. & DÉRAMOND,  
970 J. 2001. Thrust-related, diapiric, and extensional doming in a frontal orogenic wedge:  
971 Example of the Montagne Noire, Southern French Hercynian Belt. *Journal of*  
972 *Structural Geology*, **23**, 1677–1699, doi:10.1016/S0191-8141(01)00021-9.

973



974 STOCKMAL, G. S., BEAUMONT, C., NGUYEN, M. & LEE, B. 2007. Mechanics of thin-  
975 skinned fold-and-thrust belts: Insights from numerical models. *In*: SEARS, J.W.,  
976 HARMS, T. A. & EVENCHICK, C. A. (eds) *Whence the Mountains? Inquiries into the*  
977 *evolution of orogenic systems: A volume in Honor of Raymond A. Price*. Geological  
978 Society of America, Special Paper, **433**, 63–98.

979

980 STORTI, F. & MCCLAY, K. 1995. Influence of syntectonic sedimentation on thrust  
981 wedges in analogue models. *Geology*, **23**, 999-1002.

982

983 SUTTON, J. & WATSON, J. V. 1986. Architecture of the continental lithosphere.  
984 *Philosophical Transactions of the Royal Society, London*, **A317**, 5–12.

985

986 TIKOF, B. & PETERSON, K. 1998. Physical experiments of transpressional folding.  
987 *Journal of Structural Geology*, **20**, 661-672

988

989 VAN DEN DRIESSCHE, J. & BRUN, J. P. 1992. Tectonic evolution of the Montagne  
990 Noire (french Massif Central): a model of extensional gneiss dome: *Geodinamica*  
991 *Acta*, **5**, 85–99.

992

993 WEBB, A. A. G., YIN, A., HARRISON, T. M., CELERIER, J. & BURGESS, W. P. 2007. The  
994 leading edge of the Greater Himalayan Crystalline complex revealed in the NW  
995 Indian Himalaya: Implications for the evolution of the Himalayan orogen, *Geology*,  
996 **35**, 955–958, doi:10.1130/G23931A.1.

997

998 WEBB, A. A. G., SCHMITT A. K., HE, D. & WEIGAND E.L. 2011. Structural and

999 geochronological evidence for the leading edge of the Greater Himalayan Crystalline  
1000 complex in the central Nepal Himalaya. *Earth and Planetary Science Letters*, **304**,  
1001 483–495.

1002

1003 ZULAUF, J. & ZULAUF, G. 2004. Rheology of plasticine used as rock analogue: the  
1004 impact of temperature, composition and strain. *Journal of Structural Geology*, **26**,  
1005 725–737.

1006

1007 **Figures and Captions**

1008

Experiment name	Total shortening (cm)	Protowedge		Lower plate		Decollement position* (cm)	Plastiline			Erosion		
		Length (cm)	Slope (°)	Total thickness (cm)	Termination		Present	Thickness (cm)	Position* (cm)	Present	Start† (cm)	Slope
<b>Exp 1</b>	150	61	7	3.1	Straight	Top lower plate	No			No		
Exp 2	150	66	4	3.1	Straight	Top lower plate	No			No		
Exp 3	160	80	2	3.1	Gradual	Top lower plate	No			No		
<b>Exp 4</b>	180	74	0	3.1	Straight	1.1	No			No		
<b>Exp 5</b>	201	74	0	3.1	Straight	1.1	No			Yes	30	Variable
<b>Exp 6</b>	198	66	4	3.1	Straight	2.1	No			Yes	30	Variable
Exp 7	220	66	4	3.1	Straight	2.1	No			Yes	20	Fixed (5°)
Exp 8	160	80	2	3.3	Gradual	Top lower plate	Yes	0.3	1.7	No		
Exp 9	167	90	0	3.3	Gradual (-15cm)‡	Top lower plate	Yes	0.2	1	No		
<b>Exp 10</b>	163	90	0	3.3	Gradual (-15cm)‡	Top lower plate	Yes	0.1	1	No		
<b>Exp 11</b>	193	90	0	3.3	Gradual (-15cm)‡	Top lower plate	Yes	0.1	1	Yes	25	Fixed (5°)
Exp 12	175	80	2	3.3	Gradual	1.48	Yes	0.2	1.5	No		
<b>Exp 13</b>	200	90	0	3.5	Gradual (-15cm)‡	1	Yes	0.1	1.7	Yes	15	Fixed (3°)

Notes:

\* Height from base plate

† Amount of initial shortening without erosion

‡ Lower plate ends before the backstop

1009

1010 **Table 1.** *Parameters used for the thirteen experiments.* (Models described in the text are in bold)

1011

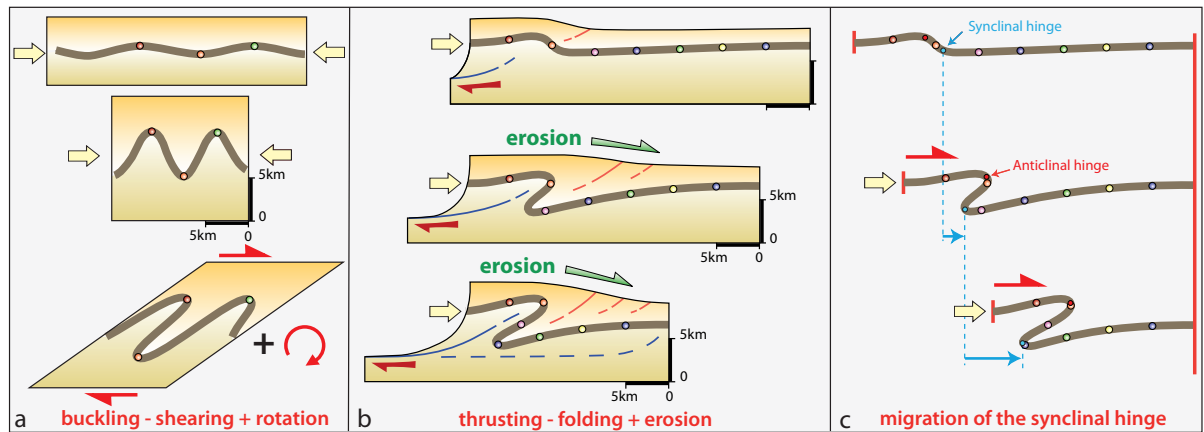


Fig. 1.

1013  
 1014 **Fig. 1.** Cartoon showing two folding mechanisms to generate large-scale overturned  
 1015 folds in fold and thrust belts. The first mechanism involve an important burial  
 1016 whereas the second one allows the development of large folds with slight burial. (a)  
 1017 Buckling and folding during compressional shortening followed by shearing and  
 1018 tilting of fold limbs; (b) Fold amplification by thrusting and subsequent shearing,  
 1019 unrolling and migration of the synclinal hinge in the frame of a fold and thrust wedge;  
 1020 (c) Simplified kinematic sketch of the same process. Coloured circles are passive  
 1021 markers regularly spaced in the folded layer.

1022

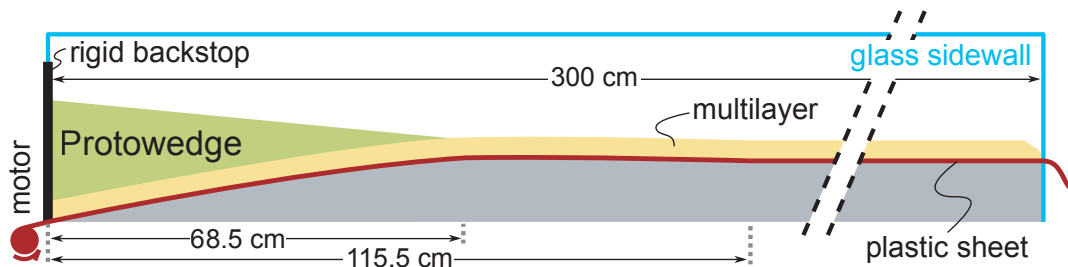
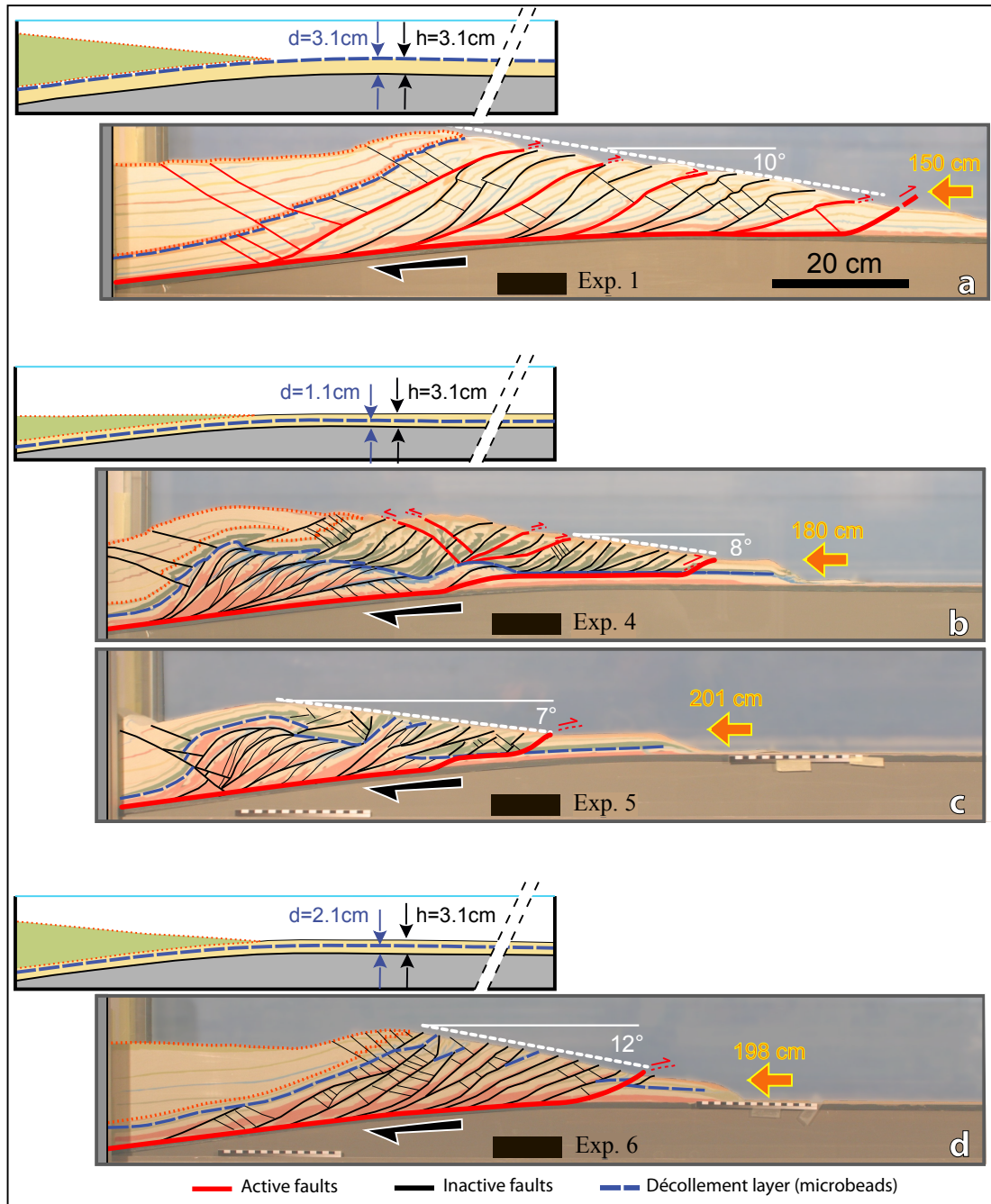


Fig. 2

1023  
 1024 **Fig. 2.** Experimental set-up. The width of the device is 10 cm.

1025



1026

1027

1028

1029

1030

1031

1032

Fig. 3

**Fig. 3.** Initial configuration and final result of models involving a microbeads layer

located at different heights (“d” on sketch). (a) Classical high friction thrust wedge.

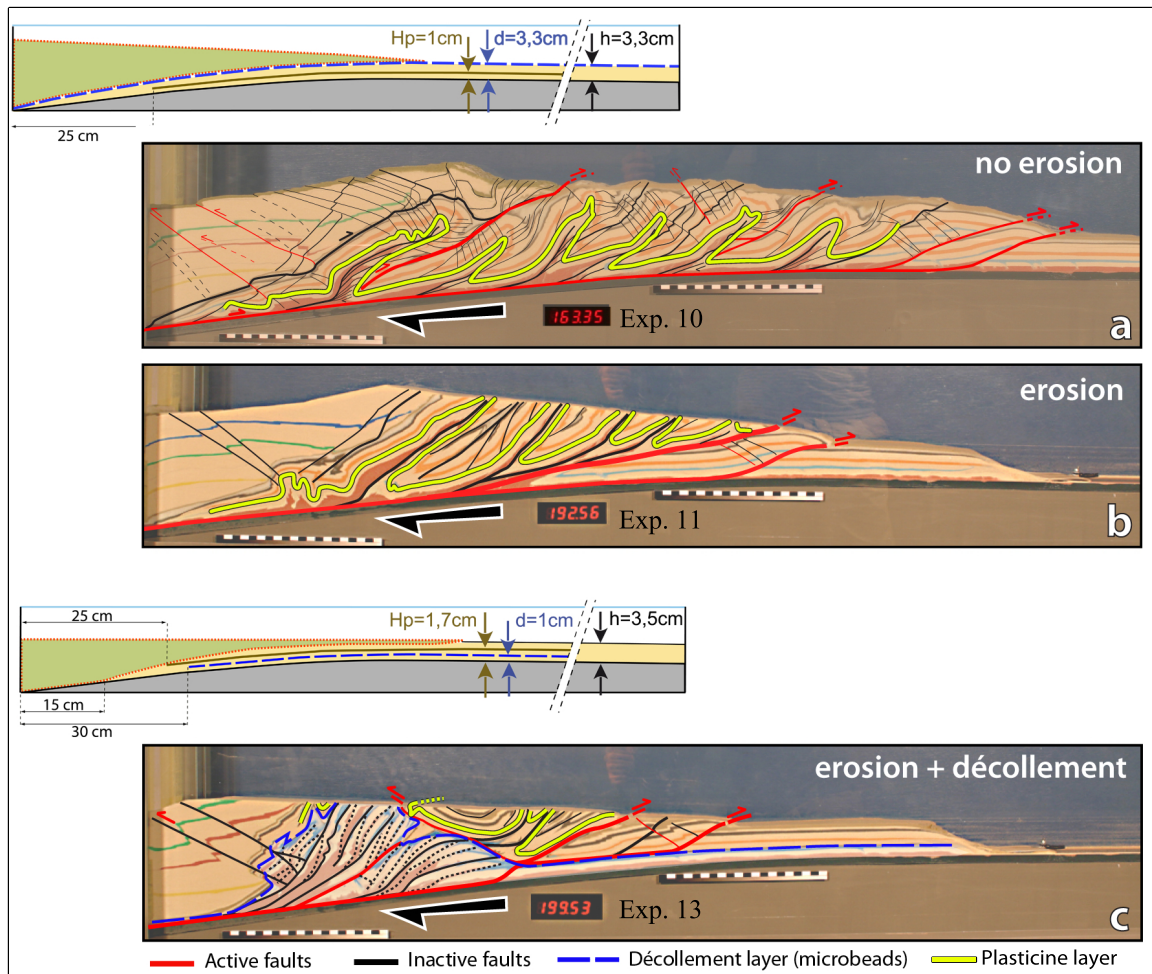
The thrust front propagates in a piggy-back style, but some faults remain active after

the nucleation of new faults at the front. (b) Strain partitioning: duplexing at the base

of the wedge and frontal accretion at the toe. Note the cyclical behavior of

underplating. (c) Impact of surface erosion on the wedge dynamics, location of

1033 underplating and exhumation of underplated units. (d) Underplating is inhibited when  
 1034 décollement is too shallow. Shortening in cm on digital screen.  
 1035



1036 **Fig. 4.** Initial setting and final stage of model involving a thin layer of plasticine ( $H_p$ :  
 1037 Height of the plasticine layer on sketch). (a) Case no erosion. Folds are overturned  
 1038 with an angle between  $30^\circ$  and  $50^\circ$ ; (b) Same experiment with erosion; (c)  
 1039 Brittle/plastic model with décollement layer and erosion. Shortening in cm on digital  
 1040 screen.  
 1041  
 1042

Fig. 4

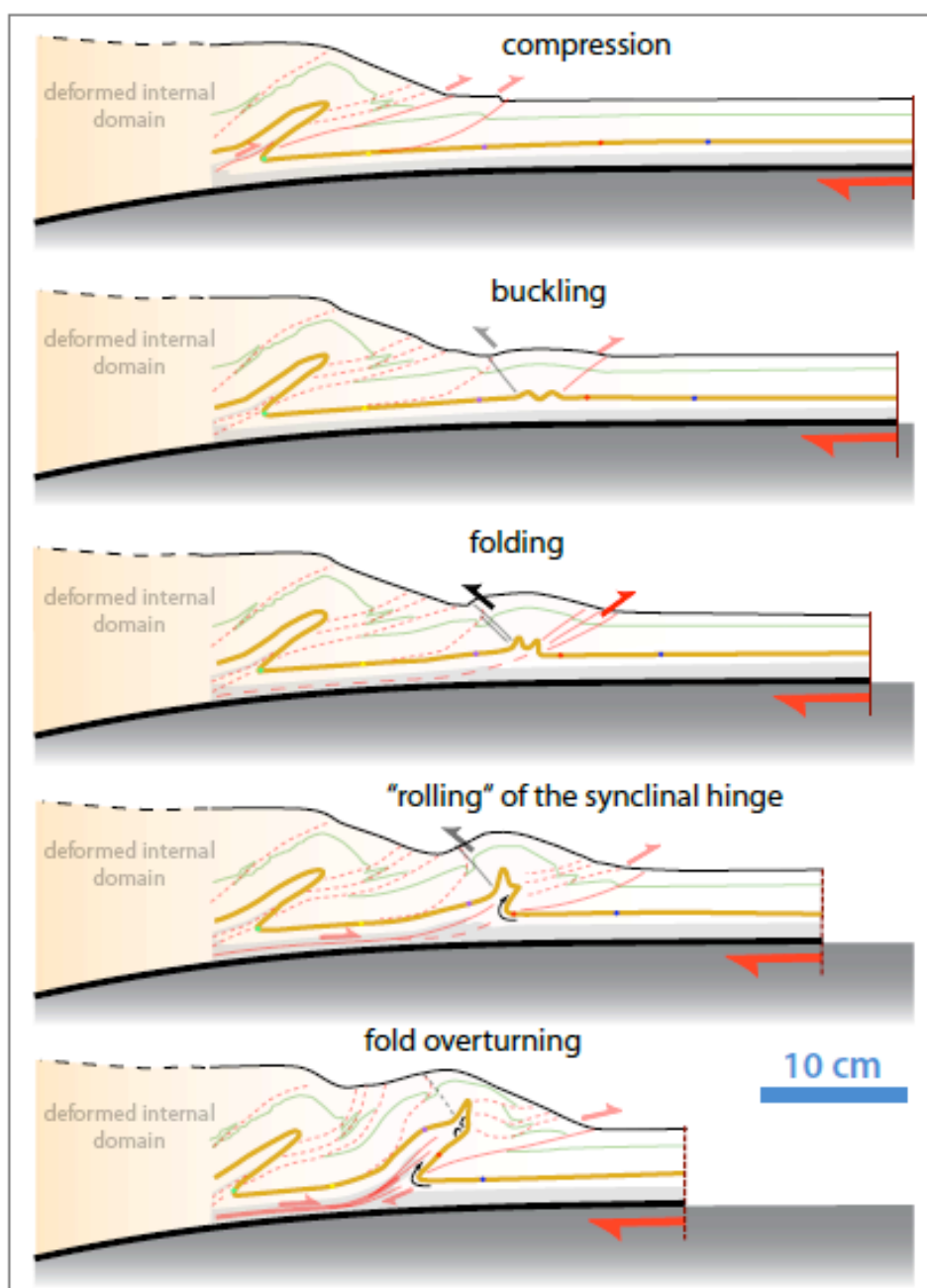


Fig. 5

1043

1044 **Fig. 5.** Kinematic model of folding. The thick line with circles represents the  
 1045 plasticine with displacement indicators.

1046

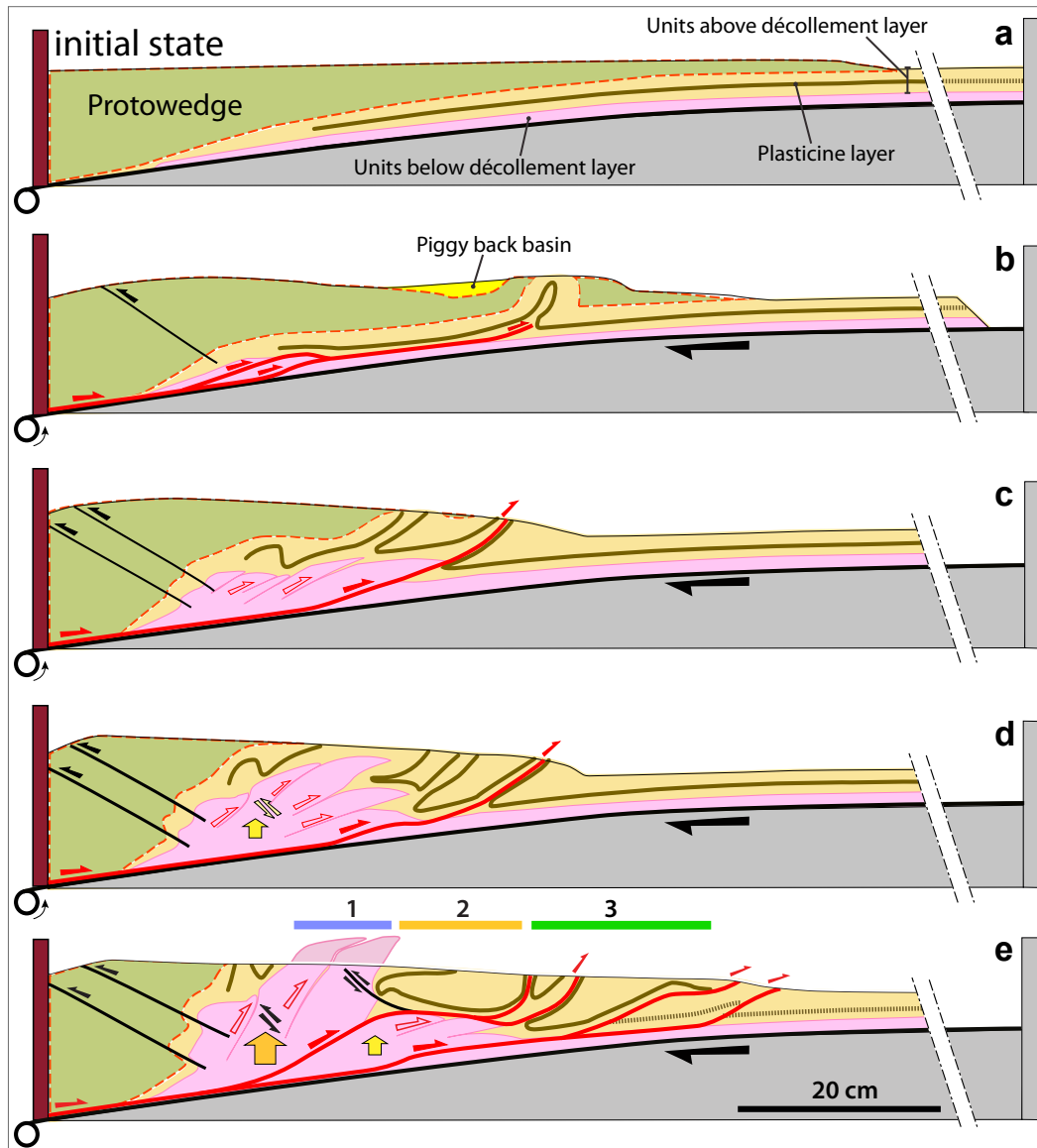


Fig. 6

1047

1048

**Fig. 6.** Evolution of complex model involving brittle/plastic multilayer, erosion and

1049

décollement layer. Upper units situated above décollement layer are composed of

1050

sand and plasticine; deep units below décollement layer are composed of sand. At the

1051

final stage (e), three domains are juxtaposed: (1) exhumation of deep rocks, (2) the

1052

domain of recumbent folds and (3) the overturned folds.

1053



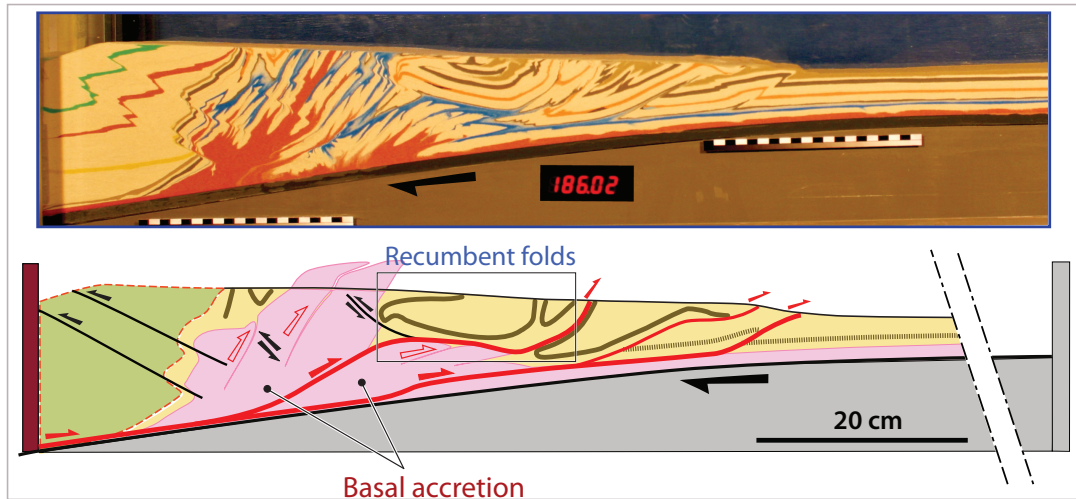


Fig.7

1054  
 1055 **Fig. 7.** Relationships between cyclical duplexing and kinematics of folding in a  
 1056 brittle/plastic model with erosion and décollement level.

1057

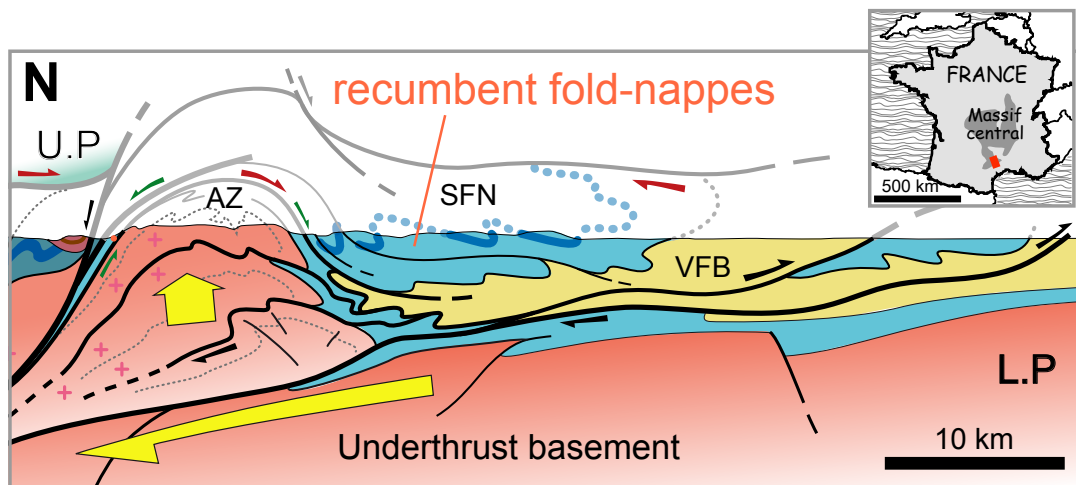


Fig.8

1058  
 1059 **Fig. 8.** Cross-section of the Montagne Noire, southern part of French Massif Central  
 1060 (modified from Malavieille 2010). U.P.: Upper Plate, L.P.: Lower Plate. AZ: Axial  
 1061 Zone, SFN: Southern Fold Nappes, VFB: Visean Foreland Basin.

1062

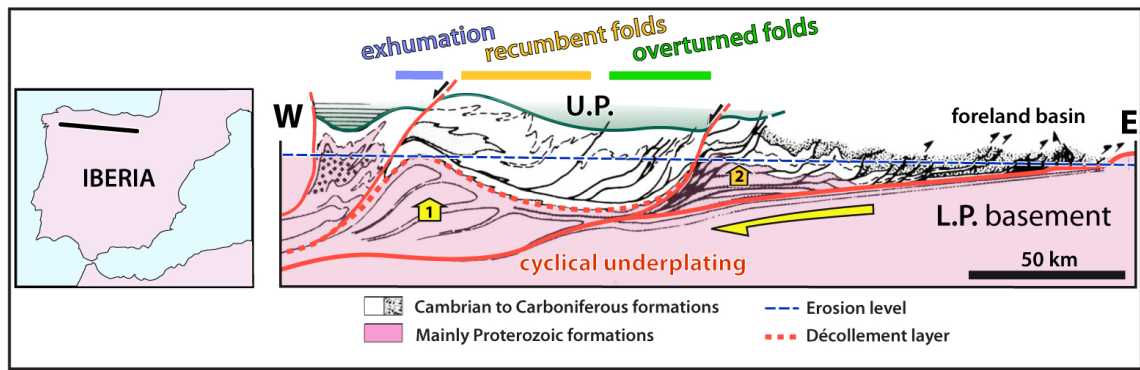


Fig.9

1063

1064 **Fig. 9.** Cross-section of Variscan Belt in Galicia, Spain (modified from Pérez-Estàun  
 1065 *et al.* 1991). U.P.: Upper Plate; L.P.: Lower Plate.

1066

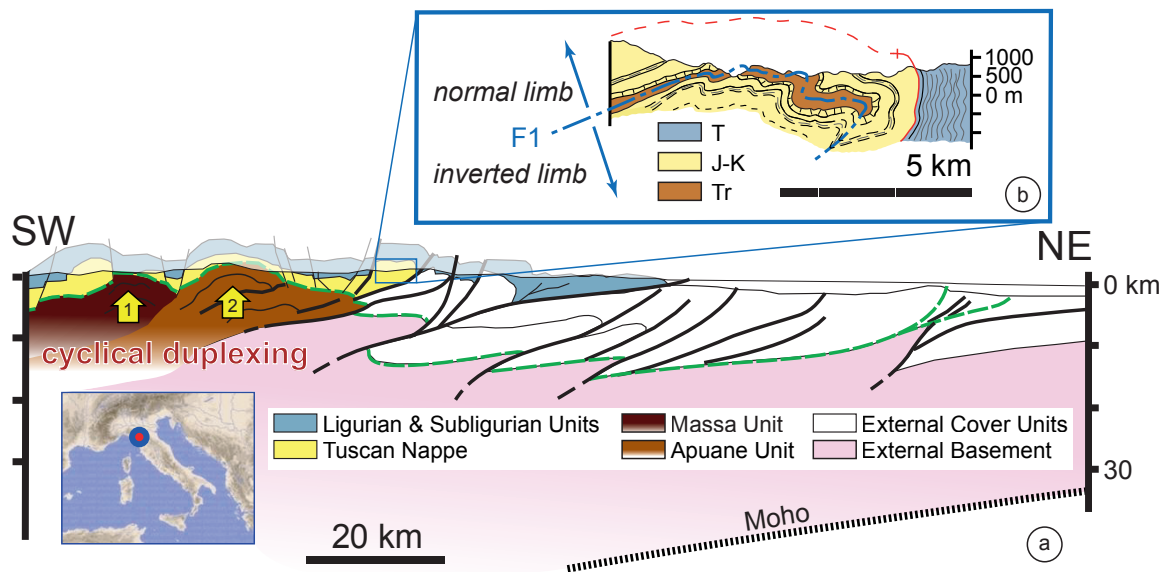


Fig. 10

1067

1068 **Fig. 10.** (a) Cross section of the Northern Apennines, Italy (modified from Molli  
 1069 2008). (b) Cross-section of the Val di Lima fold structure (modified from Baldacci *et*  
 1070 *al.* 1992). T: Tertiary; J-K: Jurassic-Cretaceous; Tr: Triassic.

1071